Provided for non-commercial research and educational use only.
Not for reproduction or distribution or commercial use.

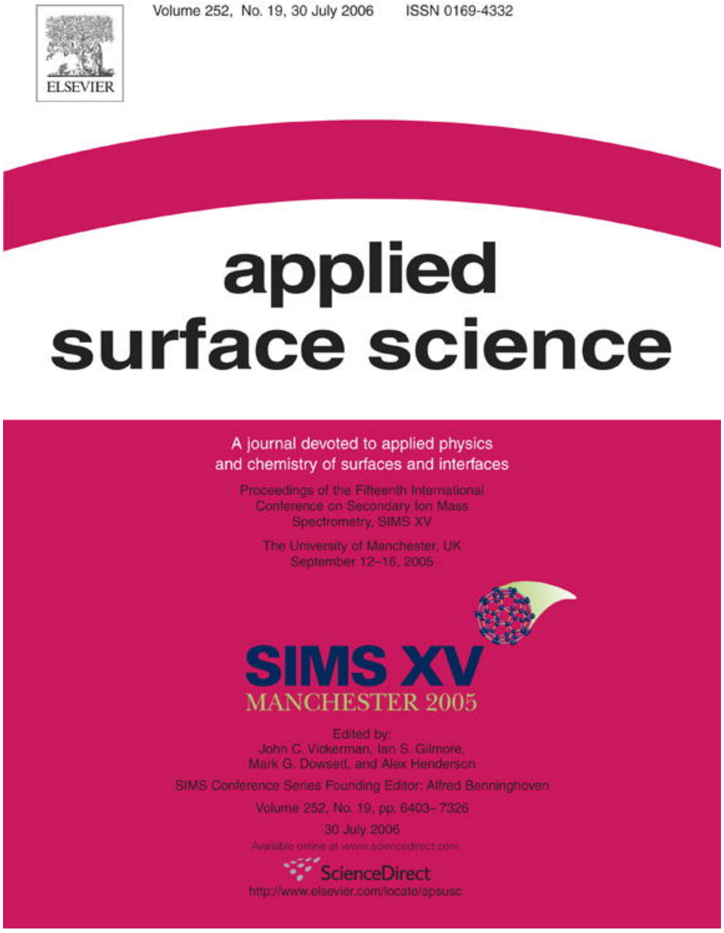

Volume 252, No. 19, 30 July 2006 ISSN 0169-4332

applied
surface science

A journal devoted to applied physics
and chemistry of surfaces and interfaces

Proceedings of the Fifteenth International
Conference on Secondary Ion Mass
Spectrometry, SIMS XV

The University of Manchester, UK
September 12–16, 2005

SIMS XV
MANCHESTER 2005

Edited by:
John C. Vickerman, Ian S. Gilmore,
Mark G. Dowsett, and Alex Henderson

SIMS Conference Series Founding Editor: Alfred Benninghoven

Volume 252, No. 19, pp. 6403–7326
30 July 2006
Available online at www.sciencedirect.com
ScienceDirect
http://www.elsevier.com/locate/apsusc

This article was originally published in a journal published by Elsevier, and the attached copy is provided by Elsevier for the author's benefit and for the benefit of the author's institution, for non-commercial research and educational use including without limitation use in instruction at your institution, sending it to specific colleagues that you know, and providing a copy to your institution's administrator.

All other uses, reproduction and distribution, including without limitation commercial reprints, selling or licensing copies or access, or posting on open internet sites, your personal or institution's website or repository, are prohibited. For exceptions, permission may be sought for such use through Elsevier's permissions site at:

http://www.elsevier.com/locate/permissionusematerial

Available online at www.sciencedirect.com
SCIENCE DIRECT®

Applied Surface Science 252 (2006) 6950–6956

applied surface science

www.elsevier.com/locate/apsusc

Quantitative analysis of supported membrane composition using the NanoSIMS

Mary L. Kraft [a], Simon Foster Fishel [a], Carine Galli Marxer [a], Peter K. Weber [b], Ian D. Hutcheon [b], Steven G. Boxer [a,]*

[a] *Department of Chemistry, Stanford University, Stanford, CA 94305-5080, United States*
[b] *Lawrence Livermore National Laboratory, Livermore, CA 94551, United States*

Received 12 September 2005; accepted 15 February 2006
Available online 6 June 2006

Abstract

We have improved methods reported earlier [1] for sample preparation, imaging and quantifying components in supported lipid bilayers using high-resolution secondary ion mass spectrometry performed with the NanoSIMS 50. By selectively incorporating a unique stable isotope into each component of interest, a component-specific image is generated from the location and intensity of the unique secondary ion signals exclusively produced by each molecule. Up to five species can be simultaneously analyzed. Homogeneous supported lipid bilayers that systematically varied in their isotopic enrichment levels were freeze-dried and analyzed with the NanoSIMS 50. The molecule-specific secondary ion signal intensities had an excellent linear correlation to the isotopically labeled lipid content. Statistically indistinguishable calibration curves were obtained using different sample sets analyzed months apart. Fluid bilayers can be patterned using lithographic methods and the composition of each corralled region varied systematically by simple microfluidic methods. The resulting composition variations can be imaged and quantified. This approach opens the possibility of imaging and quantifying the composition of microdomains within membranes, including protein components, without using bulky labels and with very high lateral resolution and sensitivity.

© 2006 Elsevier B.V. All rights reserved.

Keywords: Lipid; Bilayer; SIMS; NanoSIMS; Mixture; Gradient; Compositional analysis

---

1. Introduction

1.1. Motivation

The lipid bilayer is the basic assemblage common to all biological membranes. In addition to providing the principle structural motif for biological membranes, lipids are also actively involved in numerous functions, including recognition and processing of lipid head groups and side chains, and membrane fusion during viral entry, exo- and endocytosis. However, the majority of active functions associated with membranes involve integral membrane and membrane-anchored proteins.

The classic fluid-mosaic model suggests that all membrane components are freely mixing. During the past few years there has been an explosion of interest in the lateral associations and organization of membrane components that expand this concept with important functional consequences. Different lipid and protein components within membranes exhibit lateral (2D) mobility, in some cases over the entire membrane surface, whereas in others, lateral mobility is confined to domains whose origin is not well understood. The concept of microdomains within a membrane, sometimes called lipid rafts, emerged from the observation of a detergent insoluble membrane fraction enriched in cholesterol and/or sphingomyelin and associated with glycolipids such as gangliosides, GPI-tethered proteins, or proteins modified with attached saturated fatty acids [2–4]. In short order, the lipid raft hypothesis has become a generic description of lateral interactions although evidence for the existence of rafts in intact membranes, as well as their size, lifetime, and specific function is controversial. The characterization of these interactions is especially challenging since these associations are presumably dynamic and quite short range.

The lateral organization and dynamics of membrane components have been probed with numerous different methods. Utilization of fluorescence from labeled components is the most sensitive approach, and many advanced microscopy methods

---

* Corresponding author. Tel.: +1 650 723 4482; fax: +1 650 723 4817.
E-mail address: sboxer@stanford.edu (S.G. Boxer).

0169-4332/$ – see front matter © 2006 Elsevier B.V. All rights reserved.
doi:10.1016/j.apsusc.2006.02.116

have been developed to investigate interactions, including co-localization. Fluorescence resonance energy transfer (FRET) can be used to probe distances between labeled components on the order of 10 nm or less. Of course, the objects of interest must be labeled, and in the case of lipid components, these labels may interfere with the delicate interactions encountered within the membrane. Protein components can be imaged through selective binding to antibodies that are conjugated to heavy atom particles, followed by freeze-fracture and visualization by electron microscopy; however, only a few components can be imaged in this way. AFM offers excellent lateral and vertical resolution; however, the identity of imaged objects is often difficult to assess.

These general observations and limitations motivated us to employ a mass spectrometry technique with the highest possible lateral resolution to explore membrane organization. The NanoSIMS 50 (Cameca, Courbevoie, France) offers the possibility of imaging components based on the elemental or isotopic composition of their atomic and molecular ion fragments with high lateral resolution and sensitivity, yielding information that can complement other analytical methods, including many other types of SIMS experiments [5–23]. Because the membrane components are extensively fragmented, their identities must be encoded by isotopic substitution. In our first report we outlined an evolving set of methods for sample preparation and SIMS analysis [1]; these methods have been considerably refined and this is reported here and in subsequent papers [24,25].

1.2. Supported lipid bilayers

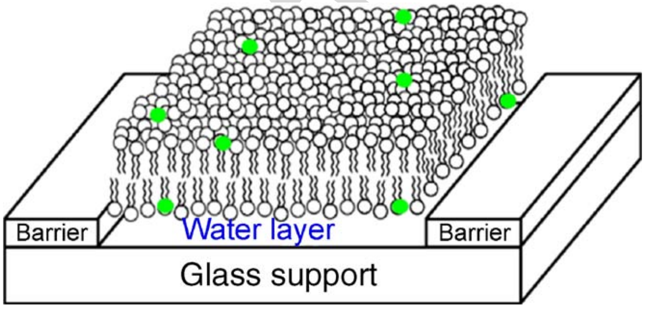

Fig. 1. Schematic diagram illustrating a supported bilayer membrane on glass patterned by a barrier [26–28]. Many materials can be used as barriers; Cr grid lines nominally 5 nm in height and 5 μm wide were used for the NanoSIMS experiments reported here.

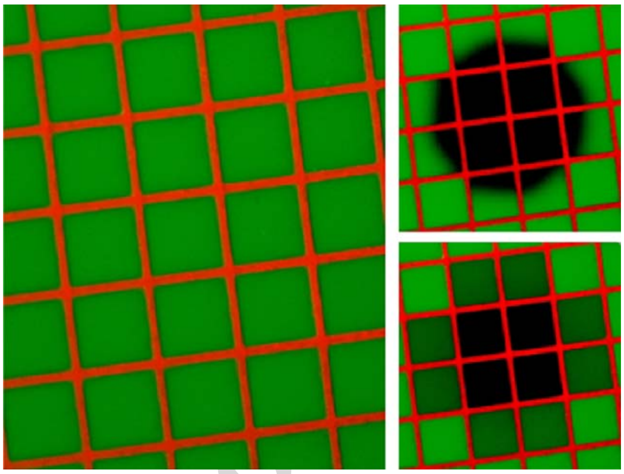

Fig. 2. A supported lipid bilayer (green) patterned by a grid of microcontact printed bovine serum albumin (red, corral size 50 μm × 50 μm), one of the many materials that can be used to create membrane corrals. A photobleached spot (black, upper right panel) relaxes (20 min later; lower right panel) demonstrating lateral fluidity, confinement and complete mixing within the corralled regions [35].

Supported lipid bilayers are created by the self-assembly of lipids into bilayers on solid supports (Fig. 1) [26–28]. Lipid membranes on solid supports, such as glass or oxidized silicon, retain the lateral fluidity associated with membranes in vesicles and in living cells [29,30]. Furthermore, living cells recognize components displayed on the surface of supported membranes [29,30]. Supported bilayers minimize non-specific interactions of proteins and cells with the solid support in contrast to bare glass or plastic substrates. The bilayer is separated from the solid support by a thin water layer approximately 1–2 nm thick [31–34]. This water lubricates the lower leaflet so that both leaflets exhibit lateral mobility. We developed the concept of membrane micropatterning, also illustrated in Fig. 1, as a means to vary and control the membrane composition [26–28]. An example demonstrating our ability to pattern these bilayers such that they retain their lateral mobility within each corralled region but cannot mix with neighboring regions is shown in Fig. 2 [35]. Many of the materials that can be patterned on glass or oxidized silicon act as barriers. We have also developed a number of methods to manipulate the lipid composition of the supported membrane confined within the corralled regions, including laminar flow patterning [36], as shown in Fig. 3 and used below. The lateral composition of supported membranes can also be altered by the application of an electric field parallel to the surface of the bilayer, which causes charged components to reorganize by a form of 2D electrophoresis [37–40].

Although these fluorescence images are useful, their lateral resolution is restricted by the diffraction limit of light and, of course, only components bearing a fluorescent label can be visualized. The planar geometry is ideal for the application of many surface analytical methods, including mass spectrometry, so long as the lateral organization can be preserved. We have previously demonstrated that NanoSIMS imaging is capable of distinguishing a lipid membrane from a protein adlayer, and also can detect compositional variations in a membrane that underwent a smooth transition from isotopically enriched to natural abundance lipid from one side of the substrate to the other [1]. Here we report refinements in sample preparation methods and steps towards obtaining quantitative information on membrane composition, which sets the stage for quantitative composition analysis of more complex membrane domains [25].

2. Experimental

2.1. Fabrication of substrates

Oxidized silicon supports for these experiments were prepared with traditional fabrication methods at the Stanford

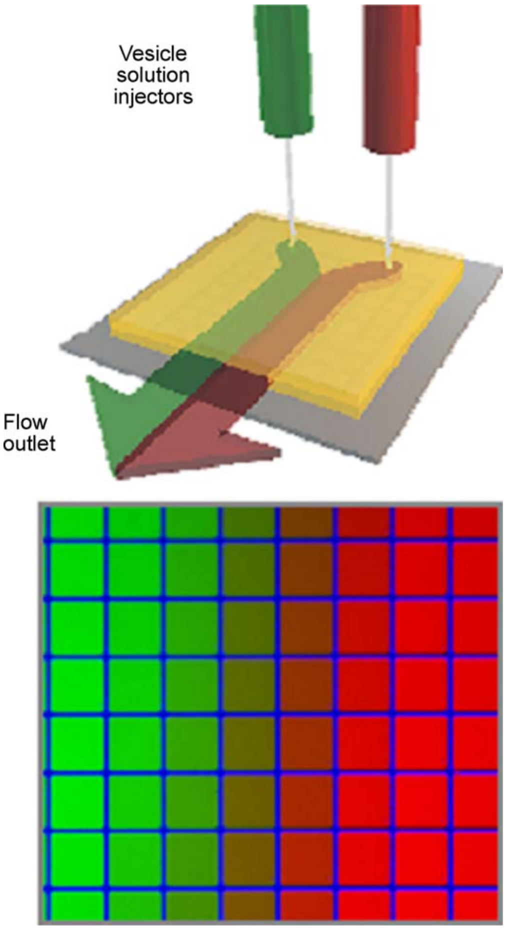

Fig. 3. Creation of a patterned membrane array by laminar flow [36]. Two streams of vesicles with different compositions (in this case green and red fluorescent lipids) are flowed in thin channels over a pre-patterned clean surface. The surface captures the composition and mixing occurs within each corral (barriers blue) to give a gradient of composition ranging from all green on the left to all red on the right.

Nanofabrication Facility. Briefly, p-type silicon wafers (Silicon Quest International, Santa Clara, CA, 4″ ⟨1 0 0⟩) were cleaned using a series of acid baths [10 min in H_2SO_4:H_2O (4:1) at 90 °C, rinse, 30 s in HF:H_2O (1:50), rinse, 10 min in H_2O:HCl:H_2O_2 (5:1:1) at 70 °C, rinse, spin dry], and oxidized in a Tylan oxidation furnace (Tystar Corporation, Torrence, CA, 17 min at 1050 °C), producing a 40 nm-thick oxide layer. This thickness of SiO_2 is a compromise between the required stability for supported membrane formation in water and charge dissipation during the NanoSIMS measurements and remains to be fully optimized. The thickness is determined by ellipsometry. Chrome grid lines to be used as corral barriers were formed on the oxidized wafers by coating the wafers with photoresist (Shipley 3612, 1.6 μm-thick), photopatterning with UV light (Karl Suss MA-6 Contact Mask Aligner) through a chrome mask of a grid (Delta Mask), selectively removing the exposed resin, and depositing a thin film of chrome (~5 nm) over the uncovered oxide and remaining photoresist. Subsequent sonication in acetone removed the photoresist and the metal that was deposited on top of it, but did not affect the chrome grid that was directly deposited on the oxidized substrate. The remaining chrome formed a grid that consisted of 5 μm-wide bars positioned 25 μm apart, thereby partitioning the surface of the oxidized substrate into a series of 20 μm × 20 μm squares. The patterned, oxidized wafers were cut into 5 mm × 5 mm squares for compatibility with the NanoSIMS sample holder using a conventional dicing saw, and cleaned by sonicating in acetone, washing with 7X detergent (ICN, Costa Mesa, CA, USA), and rinsing extensively with deionized water. We found that non-specific adhesion of vesicles to the chrome grid was greatly enhanced by annealing the substrates prior to use, therefore an annealing step was omitted in this report.

2.2. Supported lipid bilayers

1-Palmitoyl-2-oleoyl-*sn*-glycero-3-phosphocholine (POPC), 1-palmitoyl-D_{31}-2-oleoyl-*sn*-glycero-3-phosphocholine (D_{31}-POPC), and 1-palmitoyl-2-[12-(*N*-(7-nitrobenz-2-oxa-1,3-diazol-4-yl)amino)-caproyl]-*sn*-glycero-3-phosphocholine (12:0-*N*-NBD-PC) were purchased in chloroform (Avanti Polar Lipids Inc., Alabaster, AL, USA). Homogeneous lipid bilayers that systematically varied in their deuterium-enriched lipid content [0, 20, 40, 60, 80, 98 (mol)%] were employed in this study. Typically, 2 (mol)% 12:0-*N*-NBD-PC was added to each lipid mixture to facilitate evaluating the homogeneity of the membrane by fluorescence microscopy before and after freeze-drying, as this step has proven to be difficult to optimize. Ultimately there is no need to incorporate a fluorescent label, and a combination of AFM and label-free ellipsometry should suffice. The desired lipid mixtures were dissolved in chloroform, dried under a nitrogen stream, desiccated under vacuum for at least 2 h, and reconstituted with Millipore (18 MΩ) water to a concentration of 5 mg/ml. Small unilamellar vesicles were formed by passing the lipid suspension through a 50 nm-pore polycarbonate membrane 19 times. The extruded vesicles were stored at 4 °C and used within 1 week. Supported bilayers were formed by exposing the oxidized silicon substrate to the vesicle suspension, and excess vesicles were removed by rinsing in Millipore water.

2.3. Bilayer compositional gradients, droplet method

Two 2 μl droplets of an aqueous vesicle solution, each containing an isotopically distinct vesicle population (natural abundance POPC containing 2 mol% of 12:0-*N*-NBD-PC and D_{31}-POPC), were deposited on a glass coverslip such that they were separated by ~2–3 mm. A chrome-patterned substrate was placed over the droplets, causing them to come into contact with one another and begin to mix. Since membrane formation on the substrate was more rapid than the mixing of the two vesicle suspensions, the ratio of the two lipid components within the resulting bilayer varied from corral to corral. The composition within each corral was allowed to fully mix before freezing the sample.

2.4. Flow patterning

The method described in Ref. [36] and Fig. 3 was adapted to the 5 mm × 5 mm substrates used in the NanoSIMS 50. A

5 mm × 5 mm hole is cut in a thin rubber gasket such that the aforementioned silicon substrate can be placed inside with its top surface flush with that of the rubber. A small PDMS channel measuring 10 mm × 1 mm × 100 μm downstream of convergence was made by pouring the PDMS prepolymer mixture (Sylgard 184 Silicon elastomer, Dow Corning Corp., MI, USA) over a silicon master fabricated by photolithography. The rubber gasket, PDMS channel and substrate are oxidized in an air plasma for 1 min, and then sealed together, creating an enclosed channel. Holes are cored out at the outlet and both inlets. The channel is first filled with water, then the desired vesicle solutions are injected into each inlet, and a Kimwipe is placed in contact with the solution at the outlet, which serves to draw the vesicle solutions through the channel and establish the desired laminar flow conditions.

2.5. Freeze-drying

The samples were flash-frozen and freeze-dried as previously reported [1] to preserve the lateral organization of the lipid components within the membranes during NanoSIMS analysis. Briefly, the samples were carefully removed from the water such that the bilayer remained hydrated by a drop of water that remained on top of the substrate, and manually plunged into liquid ethane. The samples were transferred from the ethane into a pre-cooled drying chamber that was bathed in liquid nitrogen to keep the sample frozen throughout the drying process, and then subjected to reduced pressure (90 μbar) generated by an oil-free scroll pump (Varian Inc., Lexington, MA, USA) equipped with a liquid nitrogen trap for a minimum of 12 h.

2.6. Secondary ion mass spectrometry (SIMS)

SIMS was performed using the Lawrence Livermore National Laboratory NanoSIMS 50 in simultaneous secondary ion collection mode with pulse counting on the electron multipliers. A micro-cesium source was used to generate 16 kV Cs^+ primary ions for sample interrogation. The primary beam was tuned to a nominal spot size of ~100 nm, which determines the lateral resolution of these measurements (100 nm), with ~2 pA Cs^+, and stepped over the sample in a 256 × 256 pixel raster to generate quantitative secondary ion images. The same region was re-rastered nine times, creating a series of images, one for each raster plane, that were compiled together to create a total image, which is presented below. The dwell time was 500 μs/pixel. The magnetic field in the mass spectrometer for secondary ions was set to detect $^{31}P^-$ on the fixed electron multiplier (EM5), and the four movable electron multipliers were positioned to detect $^{12}C^-$, $^{12}C^1H^-$, $^{12}C^2H^-$, and $^{12}C^{14}N^-$. The secondary mass spectrometer was tuned for ~6800 mass resolving power to resolve isobaric interferences. The slit at the entrance of the multiplier was set at 25 μm for the resolution of $^{13}C^1H^-$ ($m/e = 14.0106$), $^{12}C^2H^-$ ($m/e = 14.0136$) and $^{12}C^1H_2{}^-$ ($m/e = 14.0151$). Samples were also simultaneously imaged using the secondary electrons that were detected by a photomultiplier. The samples were first visually located with a CCD camera, then were moved to the analysis position in the NanoSIMS 50 and precisely positioned using real-time secondary electron imaging.

2.7. Data analysis

Data analysis was performed using custom software, which runs on the PV-WAVE platform (Visual Numerics Inc., Houston, TX). The NanoSIMS 50 signals were normalized with respect to $^{12}C^-$ in order to minimize systematic signal intensity variations that arose during the measurements. Each image of the normalized $^{12}C^2H^-$ signal was smoothed with a 3-pixel window for noise reduction. As a result of the smoothing, the outer 3 pixels of each individual image appear black. Multiple individual images were assembled by aligning their overlapping regions to create a map of the isotopic enrichment within the sample. As the main purpose of this report is to document improvements in sample preparation and quantification, optimized resolution and sensitivity were not the issue; these topics will be described in subsequent publications [24]. To establish calibration curves, several regions of interest were selected on each homogeneous sample of a specified (mol)% D_{31}-POPC such that it contained the area covered by membrane within a single grid box, but did not include secondary ion signals originating from the chrome grid or obvious defects in the bilayer (see, for example, Fig. 5). The normalized $^{12}C^2H^-$ signal ($^{12}C^2H^-/^{12}C^-$) was determined for each region using the software, which smoothed the data with a three-pixel window for noise reduction. The data for each (mol)% of D_{31}-POPC was tabulated, and the mean value for each (mol)% of D_{31}-POPC was determined using standard statistical analysis methods, where the range for the average value was tabulated to the 95% confidence level. The best-fit line was determined by linear regression. For the estimation of the (mol)% of D_{31}-POPC in the gradient samples, regions of interest were selected as described above, and the concentration of D_{31}-POPC in each isolated membrane encircled by grid bars was derived from the normalized $^{12}C^2H^-$ signal from that area using the calibration.

3. Results and discussion

The absence of foreign material in the bilayer region is imperative to establishing reproducible calibration curves. Therefore we employed chrome grids, which, unlike microcontact-printed protein grids [1,14], are completely insoluble in water. Grids are important not only because of the corralling illustrated in Fig. 2 and in the gradients described below, but because they provide convenient landmarks on the surface; these are especially important when comparisons between NanoSIMS, fluorescence and AFM images are desired [1,25]. In addition, we found that the use of chrome barriers, in conjunction with the substitution of 12:0-*N*-NBD-PC in place of Texas red-labeled lipids for visualization greatly reduced the incidence of defects in the freeze-dried samples, common in our original work [1], but now quite rare.

Homogeneous supported lipid bilayers that systematically varied in their deuterium-enriched lipid (D_{31}-POPC) content were formed on the chrome-patterned oxidized silicon

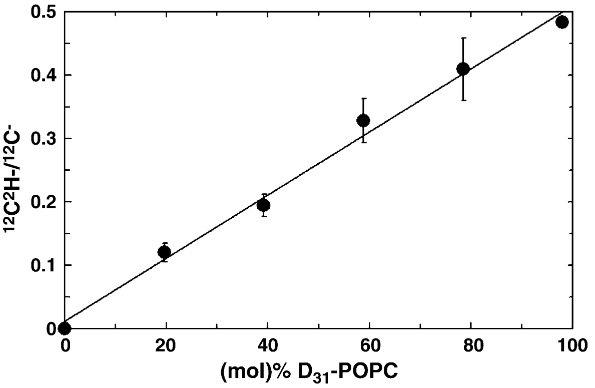

Fig. 4. Homogeneous supported lipid bilayers that systematically varied in the deuterium-enriched lipid content were freeze-dried and examined with the NanoSIMS 50. The normalized $^{12}C^2H^-$ secondary ion signal intensity ($^{12}C^2H^-/^{12}C^-$) had an excellent linear correlation with the amount of D_{31}-POPC in the membrane. The ranges for the average values were calculated with standard statistical analysis methods to the 95% confidence level are represented by the error bars. The best-fit line, determined by linear regression, was $y = 0.005x + 0.0119$.

substrates. The samples were freeze-dried and examined with the NanoSIMS 50, employing the $^{12}C^2H^-$ secondary ion signal as a gauge of the deuterium enrichment. To obtain quantitative information, the $^{12}C^2H^-$ signal must be expressed as a ratio of another secondary ion signal. In principle, this process establishes a relationship between the $^{12}C^2H^-$ signal and an internal standard, and minimizes noise by negating the spatially variant signal intensity fluctuations that result from systematic errors. The secondary ion signal of another isotope of the same element is commonly employed as the internal standard reference, for example, $^{12}C^{15}N^-/^{12}C^{14}N^-$. However, we found that normalizing $^{12}C^2H^-$ with $^{12}C^1H^-$ did not produce a reproducible linear correlation with the known D_{31}-POPC content in the bilayers. Based on our previous observation that the background signal for $^{18}O^-$ from the natural abundance of oxygen-18 (0.2%) in the oxidized silicon substrate is too high for the use of oxygen-18 as a label for membrane components [1], we believe that the $^{12}C^1H^-$ signal originated from not only the lipid membrane, but also the surface contamination and underlying substrate as well. Because the amount of surface contamination can vary among samples, the $^{12}C^1H^-$ signal is not a satisfactory internal standard. Although surface contamination is also expected to produce $^{12}C^-$ secondary ions, $^{12}C^-$ was experimentally determined to be an appropriate internal standard (see below). Carbon is a common contaminant in silicon wafers introduced throughout the substrate fabrication process [41]. Although there may be wafer-to-wafer variations, the level is expected to be quite constant across the surface of our 5 mm × 5 mm chips, and this provides a standard. This issue of internal standards is central to moving beyond imaging towards quantification and will be discussed in more detail elsewhere [24].

The normalized $^{12}C^2H^-$ signal ($^{12}C^2H^-/^{12}C^-$) acquired from the calibration sample set is displayed in Fig. 4. A linear regression was applied to the data to obtain the best-fit line: $y = 0.005x + 0.0119$ ($R^2 = 0.9924$) where y is the normalized $^{12}C^2H^-$ signal and x is the known (mol)% D_{31}-POPC in the bilayer. The normalized $^{12}C^2H^-$ secondary ion signal intensity had an excellent linear correlation with the amount of deuterium-enriched lipid within the sample. Calibration curves that were statistically indistinguishable have been obtained for separate sample sets analyzed with the NanoSIMS under the same instrumental parameters many months apart, demonstrating the reproducibility of this approach.

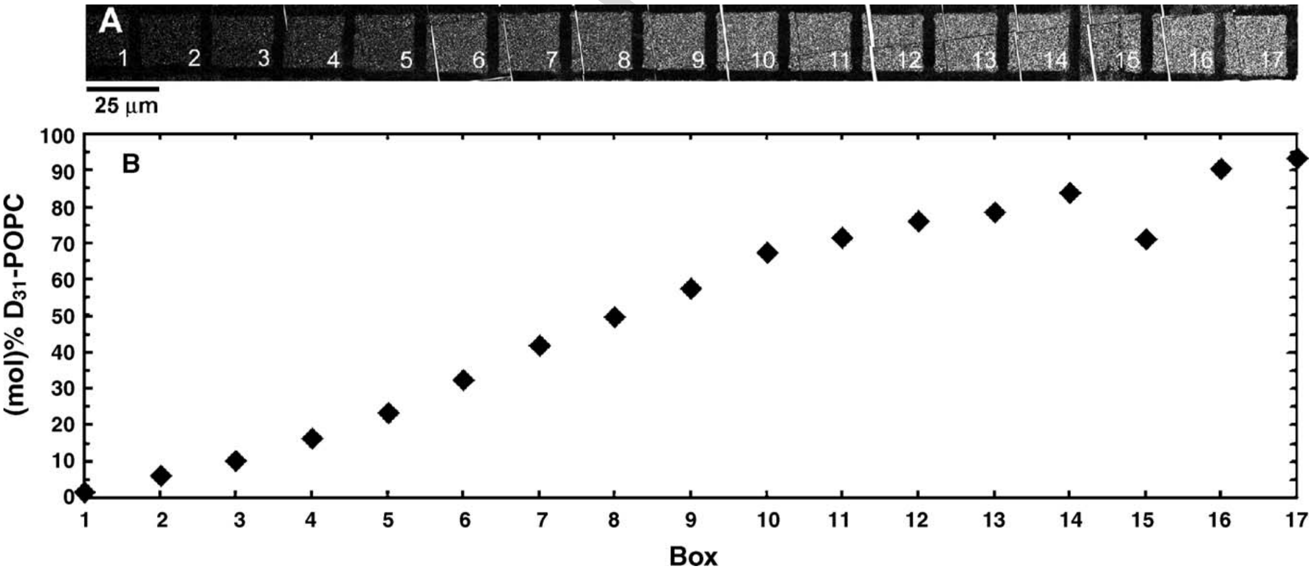

Fig. 5. NanoSIMS 50 analysis of a bilayer that contained a spatial variation in isotopic composition. A gradient between natural abundance POPC (containing 2 mol% of a fluorescent lipid for visual identification of the gradient) and D_{31}-POPC was formed by depositing one droplet of each of the two corresponding vesicle suspensions onto a chrome-patterned oxidized silicon substrate. (A) NanoSIMS images of the normalized $^{12}C^2H^-$ signal intensity revealed a transition between natural abundance (black) and deuterium-enriched lipid (white). A scratch on the substrate created visible defects in the bilayer (column that includes box 15). Multiple 25 μm × 25 μm measurements (256 × 256 pixels) were assembled to create this image. (B) Graph of the D_{31}-POPC content in the bilayer within each numbered grid box that corresponded to the average normalized $^{12}C^2H^-$ signal collected from the area. The scratch that passes through box 15 removed some of the lipid material, which is indicated by the measured D_{31}-POPC value.

This calibration curve was used to obtain quantitative chemical information on lipid membranes composed of simple compositions. Two droplets of different vesicle solutions, one composed of D$_{31}$-POPC and the other of natural abundance POPC and 2 (mol)% of a fluorescent lipid for assessing the quality of the membrane after freeze-drying, were deposited on a patterned substrate resulting in corralled bilayer regions of increasing deuterium concentration from one side of the substrate to the other. NanoSIMS secondary ion (normalized ${}^{12}C^{2}H^{-}$) images of a freeze-dried lipid bilayer that contained a compositional gradient are shown in Fig. 5A. A scratch, which forms a physical defect in the bilayer, is visible in the ion image in the corral labeled 15 and this is reflected in the quantitative analysis. Qualitatively, these images indicate that, from left to right, the deuterium-enrichment shifts from low to high. However, using the calibration curve derived from Fig. 4, a quantitative analysis of the secondary ion signals also enables the amount of D$_{31}$-POPC in the membrane to be determined, as shown in Fig. 5B. As suggested by the contrast in the images, the membrane was completely composed of natural abundance POPC at the left side of the image and the D$_{31}$-POPC content slowly increased up to $\sim$90% at the right side.

Laminar flow-patterning [15, Fig. 3] offers a more reproducible approach to forming lipid bilayers that contain well-defined compositional gradients. Gradient samples have been made using laminar flow-patterning, and the freeze-dried samples were analyzed with the NanoSIMS 50. Similar to the gradient samples discussed above, the average normalized ${}^{12}C^{2}H^{-}/{}^{12}C^{-}$ signal intensity collected is the membrane within each grid box demonstrates the membrane undergoes a smooth spatial transition in the isotopic composition from one side of the sample to the other (images not shown). In contrast to the droplet method, flow patterning provides precise control over the composition of different corrals and more than two components can be used.

4. Summary

We have developed an approach to obtain quantitative information on the lateral composition of isotopically labeled supported lipid bilayers with high-resolution secondary ion mass spectrometry. This relationship can be exploited to obtain quantitative information on microdomains within a membrane by creating similar calibration curves for multiple, unique, isotopically labeled components within the sample, and this has been used to analyze the composition of domains with a resolution better than 200 nm [25]. In this way, it should be possible to go beyond multi-isotope imaging, already a powerful tool introduced by the NanoSIMS, towards quantitative analysis.

Acknowledgements

M.L.K. is supported by an NIH NRSA fellowship; C.G.M. was supported by a postdoctoral fellowship from the Swiss National Science Foundation. This work is supported by grants from the NSF Biophysics program and NIH GM06930 (to S.G.B.), and the work at LLNL was performed under the auspices of the U.S. Department of Energy by the University of California, Lawrence Livermore National Laboratory under Contract W-7405-Eng-4. We thank Larry R. Nittler (Carnegie Institution of Washington) for development of the image processing software. We are grateful to the Stanford Nanofabrication Facility for fabrication and the NSF MRSEC CPIMA for analysis (ellipsometry) and support (S.F.F.).

References

[1] C. Galli Marxer, M.L. Kraft, P.K. Weber, I.D. Hutcheon, S.G. Boxer, Biophys. J. 88 (2005) 2965.
[2] D.A. Brown, E. London, J. Membr. Biol. 164 (1998) 103.
[3] D.A. Brown, J.K. Rose, Cell 68 (1992) 533.
[4] K. Simons, E. Ikonen, Nature 387 (1997) 569.
[5] D.M. Cannon Jr., M.L. Pacholski, N. Winograd, A.G. Ewing, J. Am. Chem. Soc. 122 (2000) 603.
[6] S. Chandra, Appl. Surf. Sci. 231–232 (2004) 462.
[7] T.L. Colliver, C.L. Brummel, M.L. Pachloski, F.D. Swanek, A.G. Ewing, N. Winograd, Anal. Chem. 69 (1997) 2225.
[8] M. Fartmann, C. Kriegeskotte, S. Dambach, A. Wittig, W. Sauerwein, H.F. Arlinghaus, Appl. Surf. Sci. 231–232 (2004) 428.
[9] N.P. Lockyer, J.C. Vickerman, Appl. Surf. Sci. 212–232 (2004) 377.
[10] S.G. Ostrowski, C.T. Van Bell, N. Winograd, A.G. Ewing, Science 305 (2004) 71.
[11] J.N. Quong, M.G. Knize, K.S. Kulp, K.J. Wu, Appl. Surf. Sci. 231–232 (2004) 424.
[12] N. Stelly, S. Halpern, G. Nicolas, P. Fragu, A. Adoutte, J. Cell Sci. 108 (1895).
[13] A.G. Sostarecz, C.M. McQuaw, A.G. Ewing, N. Winograd, J. Am. Chem. Soc. 126 (2004) 13882.
[14] N. Bourdos, F. Kollmer, A. Benninghoven, M. Sieber, H.-J. Galla, Langmuir 16 (2000) 1481.
[15] N. Grignon, J.J. Vidmar, F. Hillion, B. Jaillard, in: A. Benninghoven, P. Bertrand, H.N. Migeon, H.W. Werner (Eds.), Proceedings of the 12th International Conference on Secondary Ion Mass Spectroscopy, Elsevier Science, Brussels, 2000, p. 903.
[16] J.-L. Guerquin-Kern, F. Hillion, J.-C. Madelmont, P. Labarre, J. Papon, A. Croisy, Biomed. Eng. Online 3 (2004) 10.
[17] P. Hallegot, R. Peteranderl, C. Lechene, J. Invest. Dermatol. 122 (2004) 381.
[18] A.M. Kleinfeld, J.P. Kampf, C. Lechene, J. Am. Soc. Mass Spectrom. 15 (2004) 1572.
[19] C. Lechene, S. Ito, F. Hillion, Fourteenth International Conference on Secondary Ion Mass Spectrometry, San Diego, CA, 2003.
[20] M.L. Pachloski, D.M. Cannon, A.G. Ewing, N. Winograd, J. Am. Chem. Soc. 121 (1999) 4716.
[21] R. Peteranderl, C. Lechene, J. Am. Soc. Mass Spectrom. 15 (2004) 478–485.
[22] T.P. Roddy, D.M. Cannon, C.A. Meserole, N. Winograd, A.G. Ewing, Anal. Chem. 74 (2002) 4011.
[23] T.P. Roddy, D.M. Cannon, S.G. Ostrowski, N. Winograd, A.G. Ewing, Anal. Chem. 74 (2002) 4020.
[24] M.L. Kraft, P.K. Weber, I.D. Hutcheon, S.G. Boxer, in preparation.
[25] M.L. Kraft, P.K. Weber, I.D. Hutcheon, M.L. Longo, S.G. Boxer, in preparation.
[26] S.G. Boxer, Curr. Opin. Chem. Biol. 4 (2000) 704.
[27] J.T. Groves, N. Ulman, S.G. Boxer, Science 275 (1997) 651.
[28] J.T. Groves, S.G. Boxer, Acc. Chem. Res. 35 (2002) 149.
[29] A. Grakoui, S.K. Bromley, C. Sumen, M.M. Davis, A.S. Shaw, P.M. Allen, M.L. Dustin, Nature 285 (1999) 221.
[30] M.L. Dustin, S.K. Bromley, Z. Kan, D.A. Peterson, E.R. Unanue, Proc. Natl. Acad. Sci. U.S.A. 94 (1997) 3903.

[31] S.G. Johnson, T.M. Bayerl, D.C. McDermott, G.W. Adam, A.R. Rennie, R.K. Thomas, E. Sackmann, Biophys. J. 59 (1991) 289.
[32] B.W. Koenig, S. Kruger, W.J. Orts, C.F. Majkrzak, N.F. Berk, J.V. Silverton, K. Gawrisch, Langmuir 12 (1996) 1343.
[33] T.M. Bayerl, M. Bloom, Biophys. J. 58 (1990) 357.
[34] V. Kiessling, L.K. Tamm, Biophys. J. 84 (2003) 408.
[35] L.A. Kung, L. Kam, J.S. Hovis, S.G. Boxer, Langmuir 16 (2000) 6773.
[36] L. Kam, S.G. Boxer, J. Am. Chem. Soc. 122 (2000) 12901.
[37] J.T. Groves, S.G. Boxer, Biophys. J. 69 (1995) 1972.
[38] J.T. Groves, C. Wulfing, S.G. Boxer, Biophys. J. 71 (1996) 2716.
[39] J.T. Groves, S.G. Boxer, H.M. McConnell, Proc. Natl. Acad. Sci. U.S.A. 94 (1997) 13390.
[40] J.T. Groves, S.G. Boxer, H.M. McConnell, Proc. Natl. Acad. Sci. U.S.A. 95 (1998) 935.
[41] N. Rana, P. Raghu, F. Shadman, J. Electrochem. Soc. 149 (2002) F35.